STRUCTURAL BIOLOGY

Structural basis for selective modification of Rho and Ras GTPases by *Clostridioides difficile* toxin B

Zheng Liu[1], Sicai Zhang[2], Peng Chen[1], Songhai Tian[2], Ji Zeng[2], Kay Perry[3], Min Dong[2], Rongsheng Jin[1]*

Toxin B (TcdB) is a primary cause of *Clostridioides difficile* infection (CDI). This toxin acts by glucosylating small GTPases in the Rho/Ras families, but the structural basis for TcdB recognition and selectivity of specific GTPase substrates remain unsolved. Here, we report the cocrystal structures of the glucosyltransferase domain (GTD) of two distinct TcdB variants in complex with human Cdc42 and R-Ras, respectively. These structures reveal a common structural mechanism by which TcdB recognizes Rho and R-Ras. Furthermore, we find selective clustering of adaptive residue changes in GTDs that determine their substrate preferences, which helps partition all known TcdB variants into two groups that display distinct specificities toward Rho or R-Ras. Mutations that selectively disrupt GTPases binding reduce the glucosyltransferase activity of the GTD and the toxicity of TcdB holotoxin. These findings establish the structural basis for TcdB recognition of small GTPases and reveal strategies for therapeutic interventions for CDI.

INTRODUCTION

Clostridioides difficile (formerly *Clostridium difficile*) is one of the urgent antibiotic resistance threats identified by the U.S. Centers for Disease Control and Prevention. *C. difficile* infection (CDI) causes clinical manifestations ranging from mild diarrhea to life-threatening pseudomembranous colitis, which has become the leading cause of health care–associated infective diarrhea and posed a substantial financial burden on the U.S. health system (*1*). The pathology of CDI is primarily mediated by two homologous exotoxins, toxin A (TcdA) and TcdB, which disrupt the colonic epithelium, leading to diarrhea and colitis. While the relative roles of these two toxins in the pathogenesis of CDI are not fully understood, TcdB is considered to be more virulent than TcdA as TcdB alone is capable of causing the full spectrum of diseases in humans, and $TcdA^{-}TcdB^{+}$ strains have been clinically isolated (*2*–*4*).

TcdB (~270 kDa) contains four structurally distinct domains: an N-terminal glucosyltransferase domain (GTD), a cysteine protease domain (CPD), a central transmembrane delivery and receptor binding domain (DRBD), and a C-terminal combined repetitive oligopeptides (CROPs) domain (Fig. 1A). It is widely accepted that the toxins bind to cell surface receptors and enter cells through receptor-mediated endocytosis (*2*, *5*–*8*). Acidification in the endosome triggers conformational changes in the toxins that prompt the DRBD to form a pore and deliver the GTD and the CPD across the endosomal membrane (*9*, *10*). In the cytosol, the CPD is activated by eukaryotic-specific inositol hexakisphosphate and subsequently undergoes autoproteolysis to release the GTD, which then glucosylates small guanosine triphosphatases (GTPases) in the Rho and/or Ras families (*2*, *11*–*15*).

Small GTPases are common targets of bacterial toxins (*16*). These proteins are crucial molecular switches cycling between the guanosine triphosphate (GTP)–bound active state and the guanosine diphosphate (GDP)–bound inactive state, which enable the activated GTPases to interact with many of their effector proteins and regulate diverse signal transduction pathways. The GTD of TcdB glucosylates Rho/Ras proteins at a threonine residue ($T35^{Rac1}$, $T35^{Cdc42}$, $T37^{Rho}$, and $T61^{R\text{-}Ras}$) in their switch I region using UDP-glucose as a sugar donor. Glucosylation disrupts the interactions of Rho/Ras GTPases with their downstream effector proteins and therefore abolishes signal transduction, leading to alterations in the actin cytoskeleton, cell rounding, and ultimately cell death (*11*, *17*).

TcdB variants from diverse *C. difficile* strains display different selectivity toward Rho or Ras family GTPases, which are linked to two distinct types of cytopathic effects (*14*, *18*–*20*). For example, TcdB from strains VPI10463 and UK1, which effectively modifies RhoA, Rac1, and Cdc42, but not R-Ras, causes classic rounded cells with spikes that remain attached to plates (*11*, *12*, *14*). In contrast, TcdB from strains M68, VPI1470, NAP1v, and 8864 preferentially modifies R-Ras, Rac1, and Cdc42 with a lower potency, but not RhoA, which induces perfect cell rounding and detachment (*13*, *14*, *21*, *22*). Rho and R-Ras GTPases are notably different in their sequences (~23% identity) and cellular functions: Rho GTPases are the master regulators of the cytoskeleton, cell polarity, microtubule dynamics, and intracellular traffic (*23*), while R-Ras controls the activity of integrins, cell adhesion, and vascular regeneration (*24*–*26*). The different preferences toward these two distinct GTPases by TcdB variants may contribute to the different pathogenicity in humans and animal models observed among different *C. difficile* strains (*21*, *27*).

Here, we use the GTD of TcdB from strains VPI10463 ($GTD^{VPI10463}$) and M68 (GTD^{M68}), which display distinct GTPase preferences and cytopathic effects, as examples, and report their cocrystal structures in complex with a human Cdc42 and R-Ras, respectively. Our complementary structural and functional studies reveal a common structural basis for Rho/Ras recognition shared by TcdB variants. Furthermore, we find that the GTPase-binding interfaces in the GTD provide a flexible structural platform for TcdB variants from diverse *C. difficile* strains to tune their specificity toward Rho or R-Ras, which may lead to distinct cytopathic effects in host cells.

[1]Department of Physiology and Biophysics, University of California, Irvine, Irvine, CA 92697, USA. [2]Department of Urology, Boston Children's Hospital, and Departments of Microbiology and Surgery, Harvard Medical School, Boston, MA 02115, USA. [3]NE-CAT and Department of Chemistry and Chemical Biology, Cornell University, Argonne National Laboratory, Lemont, IL 60439, USA.
*Corresponding author. Email: r.jin@uci.edu

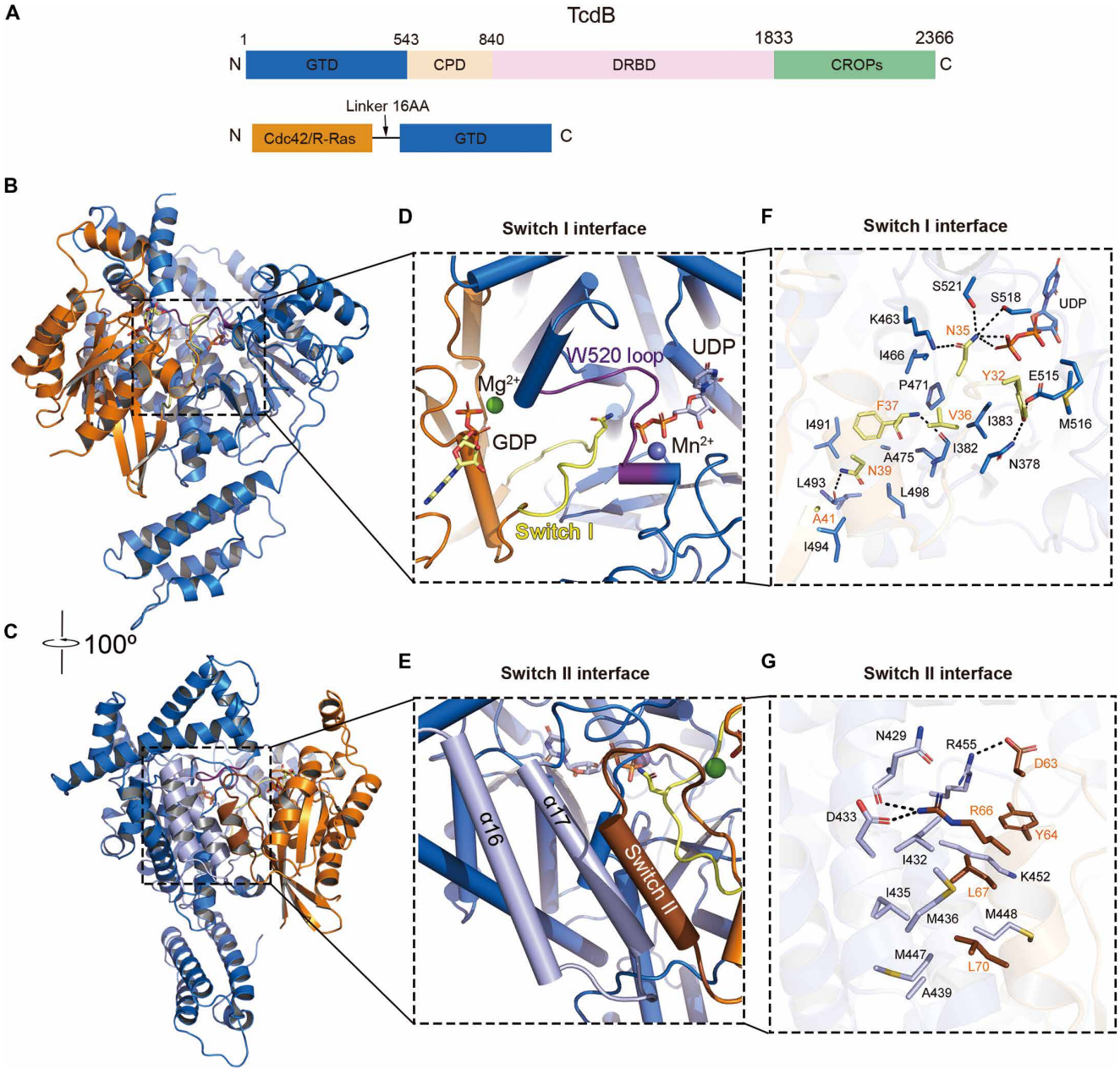

Fig. 1. Overall structure of the Cdc42–GTD^{VPI10463} complex. (**A**) A schematic diagram showing the domain organization of TcdB^{VPI10463} and the design of Cdc42–GTD^{VPI10463} and R-Ras–GTD^{M68} fusion proteins. GTD, glucosyltransferase domain (marine); CPD, cysteine protease domain (wheat); DRBD, delivery and receptor binding domain (pink); CROPs, combined repetitive oligopeptides domain (green); and Cdc42/R-Ras (orange). (**B** and **C**) Cartoon representations of the Cdc42–GTD^{VPI10463} complex with GTD^{VPI10463} colored in marine and Cdc42 in orange. (**D** and **E**) Close-up views of the interfaces: GTD^{VPI10463} W520 loop (deep purple); GTD^{VPI10463} α16–17 helices (light blue); Cdc42 switch I (yellow, residue T35N shown as sticks); and Cdc42 switch II (brown). GDP and UDP are shown as yellow and light blue sticks, respectively; Mg^{2+} and Mn^{2+} are represented as green and slate spheres, respectively. (**F** and **G**) Close-up views into the extensive interactions between Cdc42 and GTD^{VPI10463} focusing on the switch I– and switch II–binding regions.

RESULTS

The structures of the Cdc42–GTD^{VPI10463} and R-Ras–GTD^{M68} complexes

Our earlier efforts to determine the structures of the GTD in complex with Rho or Ras GTPases were hampered by the transient interactions between them, which are a common feature for most enzyme-substrate pairs. We first managed to determine a low-resolution partial structure of a RhoA–GTD^{VPI10463} complex at about 4-Å resolution after numerous trials of crystallization optimization and crystal diffraction screening at the synchrotron. This structure revealed the relative positioning of these two proteins with the C terminus of RhoA located in close proximity to the N terminus of the GTD, which is similar to an earlier model proposed based on mutagenesis study (*12*). Guided by this structure, we designed and biochemically characterized a series of tandem Rho–GTD^{VPI10463} fusion proteins, where the GTD was covalently

linked to the C terminus of RhoA, Cdc42, or Rac1 with a flexible peptide linker without restricting their interactions. Covalent linking of two proteins increases their local concentrations and thus strengthens the protein-protein interactions (*28*, *29*).

The best crystals were obtained using a Cdc42–GTD^{VPI10463} fusion protein, where GTD^{VPI10463} (residues M1–S542) and Cdc42 (residues I4–P182) were covalently linked via a 16–amino acid peptide linker (Fig. 1A). We also introduced a mutation in Cdc42 switch I (T35N) to prevent glucosylation to stabilize the complex (*11*). The best diffraction data at 2.79-Å resolution were obtained from a crystal of the Cdc42–GTD^{VPI10463} complex in the presence of cofactors for the GTD (UDP-glucose and Mn^{2+}) and Cdc42 (GDP and Mg^{2+}) (Fig. 1, B and C, and table S1). There is one pair of the Cdc42–GTD^{VPI10463} complex in an asymmetric unit with a total buried molecular interface of ~1539 Å^2. The UDP-glucose molecule in the complex was hydrolyzed, and the electron density for the UDP moiety is well defined. However, no visible electron density was observed for the cleaved glucosyl moiety of UDP-glucose or the flexible 16-residue peptide linker.

Cdc42 in the complex adopts the classic Rho GTPase fold. Most of its interactions with GTD^{VPI10463} are mediated by its switch I and switch II regions (residues 30 to 40 and 59 to 73, respectively), which otherwise act as a molecular switch modulating its interactions with effector proteins. The overall structure of the Cdc42•UDP-bound GTD^{VPI10463} is similar to the standalone GTD in the presence of UDP and glucose [Protein Data Bank (PDB): 2BVL] (*30*) or a nonhydrolyzable UDP-glucose homology U2F (PDB: 5UQN) (fig. S1A) (*31*). We notice that a loop connecting the α20 and α21 helices (W520 loop, residues 515 to 523) of the GTD displays a large conformational change in comparison to the apo GTD in all three structures with the Cα of W520 moving ~9.6 Å (fig. S1, B and C), which is believed to be triggered by its direct interactions with UDP-glucose and Mn^{2+} (*31*–*33*). In the Cdc42–GTD^{VPI10463} complex, the conformation of this W520 loop is further stabilized by residue Y32 and the T35N mutation on the switch I of Cdc42 (Fig. 1F). In contrast, the W520 loop in the apo conformation may clash with Cdc42, suggesting that UDP-glucose binding helps the GTD to engage its substrate.

Using a similar strategy, we also successfully determined the cocrystal structure of GTD^{M68} in complex with R-Ras^{T61N} in the presence of UDP-glucose, GDP, Mn^{2+}, and Mg^{2+} at 2.34-Å resolution (Fig. 2, A and B, and table S1). The overall architecture of the R-Ras–GTD^{M68} complex is very similar to the Cdc42–GTD^{VPI10463} complex, where GTD^{M68} grips R-Ras mainly through its switch I and II regions, and the W521 loop of GTD^{M68} (equivalent to the W520 loop of GTD^{VPI10463}) adopts the UDP-glucose•Mn^{2+}-bound conformation and facilitates R-Ras binding (Fig. 2, C and D, and fig. S1, D to F) (*34*). However, we observe a unique feature that is not observed in the Cdc42–GTD^{VPI10463} complex, where a region between the switch I and II of R-Ras involving residues T67, I69, R78, and D80 (termed inter-switch) is bound by GTD^{M68} via a loop between its α19 and α20 helices (Fig. 2E). The UDP-glucose molecule in the R-Ras–GTD^{M68} complex was also hydrolyzed, and we observed a clear electron density for UDP but a weak density for the hydrolyzed glucose, indicating its low occupancy.

TcdB uses a common structural basis to recognize Rho and R-Ras

It is well accepted that the switch I of small GTPases adopts distinct conformations in the presence of GTP or GDP, which is the structural basis underlying their functions as molecular switches. In this study, the GTD-bound Cdc42 and R-Ras were crystallized in the presence of GDP. Unexpectedly, the switch I of both Cdc42 and R-Ras displays a unique conformation upon toxin binding that is different from their classic GDP-bound conformations (Fig. 3, A and B, and fig. S2) (*35*). In particular, the switch I of Cdc42 and R-Ras moves away from its GDP•Mg^{2+}-binding cleft to insert into the UDP-glucose–binding pocket of the GTD, which is stabilized by extensive protein-protein interactions between the switch I and multiple discontinuous regions in the GTD that are converged in 3D (Figs. 1F and 2C and table S2). As a result, this shift of the switch I positions the key residue T35^{Cdc42} and T61$^{R\text{-}Ras}$, the targeted residues for glucosylation, in close proximity to the UDP-glucose–binding site in the GTD (Fig. 3, A and B). For example, N35$^{Cdc42\text{-}T35N}$ moves ~6.3 Å closer to the GTD and UDP, establishing hydrogen bonding with K463, S518, and S521 of the GTD and the UDP β-phosphoryl group (Fig. 1F). However, the engineered T35N^{Cdc42} or T61N$^{R\text{-}Ras}$ does not have the hydroxyl group to accept the glucosyl unit from UDP-glucose, and therefore, the cleaved glucose cannot be located in the complexes. This previously unidentified conformation of the switch I likely represents an intermediate state where T35^{Cdc42} and T61$^{R\text{-}Ras}$ are primed to be glucosylated by the GTD. In contrast to this favorable GTD-binding conformation, the switch I of Rho/Ras in the GTP-bound conformation is located further away from the GTD when compared to the GDP-bound state, while the hydroxyl groups of the Thr residue—the glucosylation target—could be engaged in intramolecule hydrogen bonds in the GTP-bound forms (fig. S2, B to D) (*35*–*39*). These results thus provide the structural basis to understand prior observations that the GDP-bound Rho GTPases are the preferred substrates for TcdB than the GTP-bound forms (*11*).

The switch II of Cdc42 and R-Ras packs against the α16–17 helices of GTD^{VPI10463} and GTD^{M68}, respectively, involving mainly hydrophobic interactions complemented with hydrogen bonds and salt bridges (Figs. 1, E and G, and 2, B and D). The conformation of the switch II of the GTD•GDP-bound Cdc42 is almost identical to the standalone GDP-bound Cdc42 (PDB: 1AN0), while the switch II of the GDP-bound R-Ras displays a conformational change to accommodate GTD^{M68} binding (PDB: 2FN4) (Fig. 3, A and B, fig. S2E, and table S2). At the same time, the Cdc42/R-Ras switch II–binding sites in GTD^{VPI10463} and GTD^{M68} are preformed in the absence of GTPases.

A third shared GTD-binding interface is found in a region upstream of the switch I of Cdc42 (T^{24}TNKFP) and R-Ras (I^{50}QSYFV) (termed pre-switch I) (Fig. 4A), whose contribution to the GTPase function is not fully appreciated. The pre-switch I of Cdc42/R-Ras is bound by two discrete regions in the GTD that form a clamp-like motif (Fig. 4, B and C). For example, the upper and lower clamps in GTD^{VPI10463} are composed of residues 308 to 311 and 378 to 381, respectively. Together, our structural studies reveal a common strategy by which the GTD from two distinct TcdB variants recognizes their preferred substrates mostly via their characteristic switch I, switch II, and a pre-switch I region.

Another interesting finding is that both the Cdc42- and R-Ras–binding interfaces in the GTD are largely masked by the CPD in the context of the full-length TcdB holotoxin (PDB code: 6OQ5) (fig. S3A) (*34*). Therefore, the GTD is in a self-inhibited state until it is cleaved by the CPD and released from the rest of the toxin. This provides a molecular explanation for the prior observation that the glucosyltransferase activities of TcdB and TcdA increased upon autoproteolytic activation and GTD release (*33*). Furthermore, our

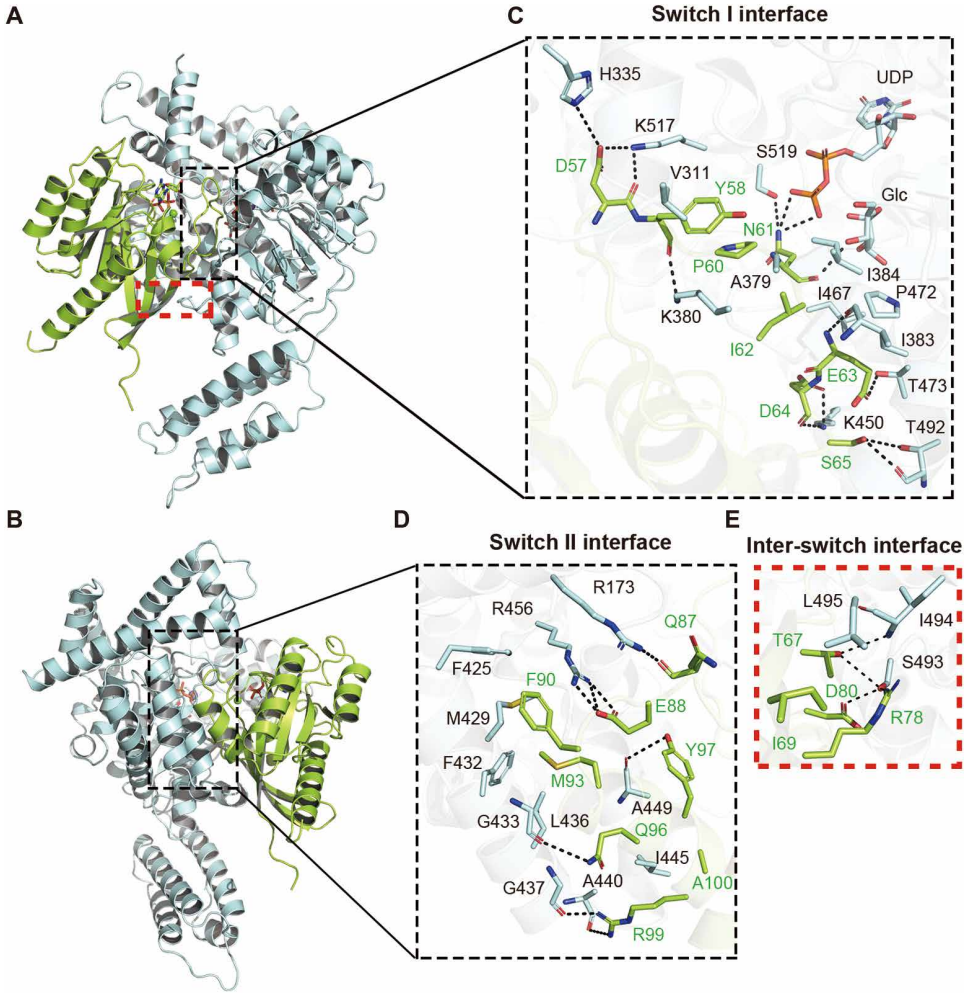

Fig. 2. Overall structure of the R-Ras–GTD^{M68} complex. (**A** and **B**) Cartoon representations of the R-Ras–GTD^{M68} complex with GTD^{M68} colored in pale cyan and R-Ras in lemon. GDP and UDP are shown as lemon and pale cyan sticks, respectively; Mg^{2+} and Mn^{2+} are represented as green and slate spheres, respectively. (**C** to **E**) Close-up views into the extensive interactions between R-Ras and GTD^{M68} focusing on the switch I, switch II, and the inter-switch in R-Ras. Interacting residues in GTD^{M68} and R-Ras are colored pale cyan and lemon, respectively.

structures also suggest that the main substrates of the GTD should be the membrane-anchored Rho GTPases (*2*, *34*), because the cytosolic Rho GTPases are predominantly bound by Rho guanosine dissociation inhibitors that occupy both the switch I and II of Rho and thus prevent GTD binding (fig. S3B) (*40*).

GTPase recognition is crucial for the cytopathic effect of TcdB

We then carried out structure-based mutagenesis studies, using GTD^{VPI10463} as a model, to validate the structural findings and better understand the functional role of the GTD in TcdB pathogenesis. Guided by the crystal structure, we designed GTD^{VPI10463} variants that carry two different types of mutations: (i) mutations that weaken GTD binding to Cdc42 switch I, including GTD^{K463G}, GTD^{I466G}, GTD^{A475D}, GTD$^{I382G/I383G}$, GTD$^{I382G/I383G/I466G}$, and GTD$^{P471G/I491G}$, and (ii) mutations in the α16–17 helices that disrupt its binding with the switch II of Cdc42, including GTD^{I432G}, GTD^{D433G}, GTD^{A439D}, GTD$^{I435G/M436G}$, and GTD$^{M447G/M448G}$. We confirmed that all these mutations did not affect GTD folding and stability based on thermal denaturation experiments (figs. S4 and S5C).

We first examined the glucosyltransferase activity of these rationally designed GTD^{VPI10463} mutants using an in vitro glucosylation assay that has been well established for Rac1 (Fig. 3C). This assay uses a monoclonal antibody (mAb 102) that is highly specific for the nonglucosylated Rac1 and another antibody mAb 23A8 that detects the total Rac1 regardless of their glucosylation states (*41*, *42*). We found that GTD^{I432G} displayed a decreased glucosyltransferase activity compared to the wild-type (WT) GTD, and the activities of GTD^{I466G}, GTD$^{I435G/M436G}$, GTD$^{M447G/M448G}$, GTD$^{I382G/I383G}$, GTD$^{P471G/I491G}$, and GTD$^{I382G/I383G/I466G}$ were further reduced (Fig. 3C and fig. S5A). On the basis of these findings, we designed another two GTD mutants, GTD^{5MA} (I382G/I383G/I466G/I435G/M436G) and GTD^{5MB} (I382G/I383G/I466G/M447G/M448G), which carry mutations to disrupt its interactions with both the switch I and switch II of Rho GTPase. As expected, the glucosyltransferase activities of these two GTD^{VPI10463} mutants were almost completely abolished (Fig. 3C and fig. S5B).

We then examined the cytopathic effect of these GTD variants using a cell-rounding assay, as inactivation of Rho GTPases by TcdB damages the actin cytoskeleton and results in the characteristic

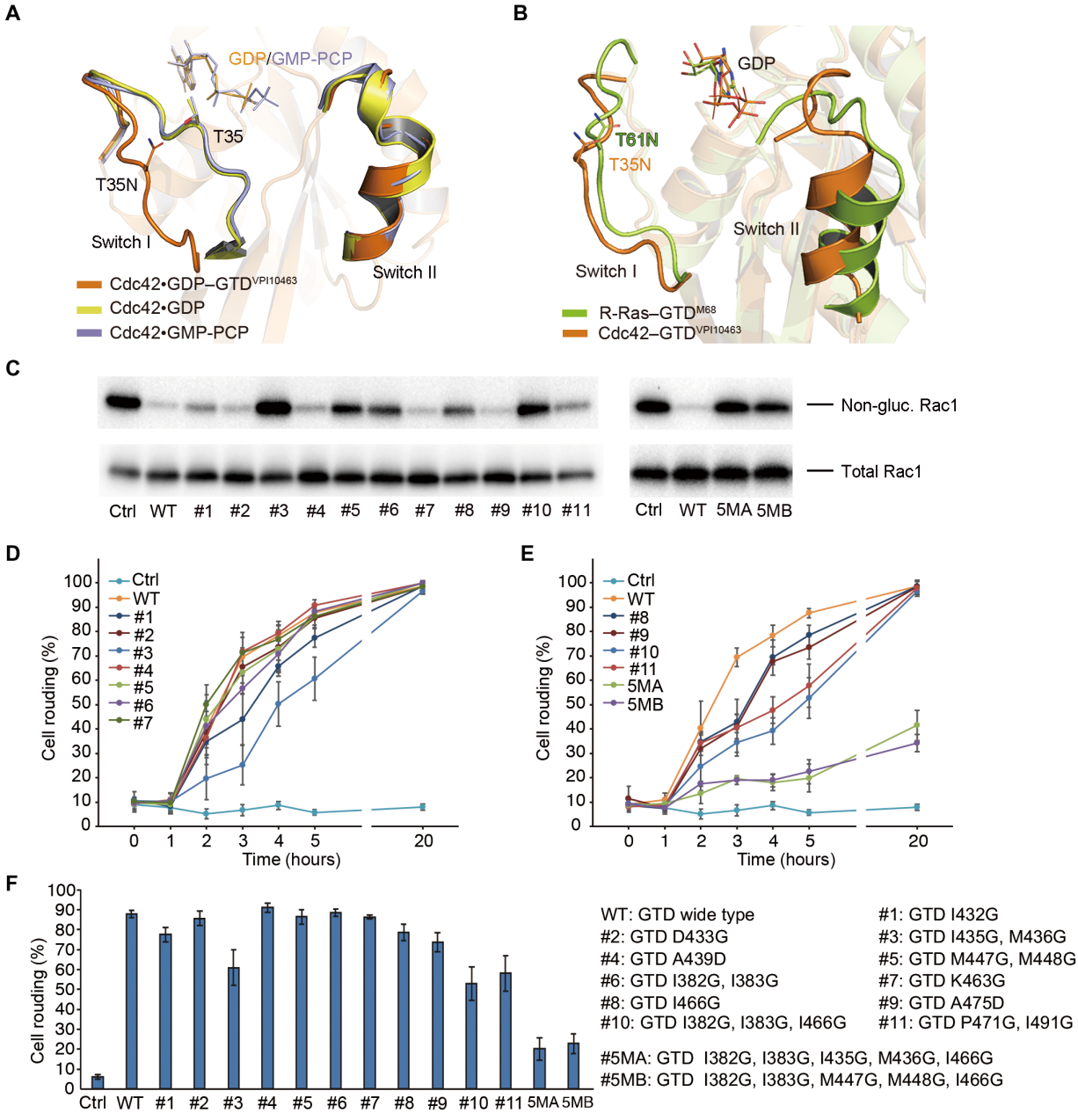

Fig. 3. GTD grips Rho/Ras mostly via their switch I and II regions, and these interactions are crucial for its cytopathic effect. (**A**) Superposition of the structures of the Cdc42•GDP–GTD^{VPI10463} complex, Cdc42•GDP (PDB: 1ANO, yellow), and Cdc42•GMP-PCP (β,γ-methyleneguanosine 5′-triphosphate) (PDB: 2QRZ, light blue) focusing on the switch I and II regions. GDP and GMP-PCP are shown as sticks. Residues T35 in the WT Cdc42 and T35N in the Cdc42•GDP–GTD complex are shown as sticks. (**B**) Structural comparison between the GTD^{M68}-bound R-Ras and the GTD^{VPI10463}-bound Cdc42, focusing on the switch I and II regions. Residues T61N$^{R\text{-}Ras}$ and T35N^{Cdc42} are shown as sticks. (**C**) The glucosyltransferase activities of the selected GTD^{VPI10463} mutants toward the recombinant Rac1 were examined using an in vitro assay. (**D** and **E**) The cytopathic effects of the GTD^{VPI10463} mutants were examined using the cell-rounding assay, and the percentage of rounded cells was quantified. (**F**) The percentages of rounded cells at 5 hours after treatment. The data are presented as means ± SD, $n = 3$.

cell-rounding phenotype (*43*). The WT GTD^{VPI10463} and its variants were delivered into HeLa cells using Lipofectamine CRISPRMAX reagents, and the percentage of rounded cells was examined. We found that GTD$^{I382G/I383G}$, GTD^{I466G}, GTD$^{I382G/I383G/I466G}$, and GTD$^{P471G/I491G}$ that have disrupted interactions with the switch I of Cdc42 and GTD$^{I435G/M436G}$ and GTD$^{M447G/M448G}$ that have corrupted switch II–binding interfaces showed notably decreased toxicity. GTD^{5MA} and GTD^{5MB} that carry mutations in both the switch I– and switch II–binding interfaces showed more than 70% decreased toxicity 5 hours after treatment and ~60% reduction after 20 hours (Fig. 3, D to F). In comparison, our negative control, the well-studied catalytically inactive GTD-N^{286}XN^{288} mutant that has a disrupted Mn^{2+}•UDP-glucose–binding pocket, was atoxic after 20 hours post-delivery (fig. S6, A and B).

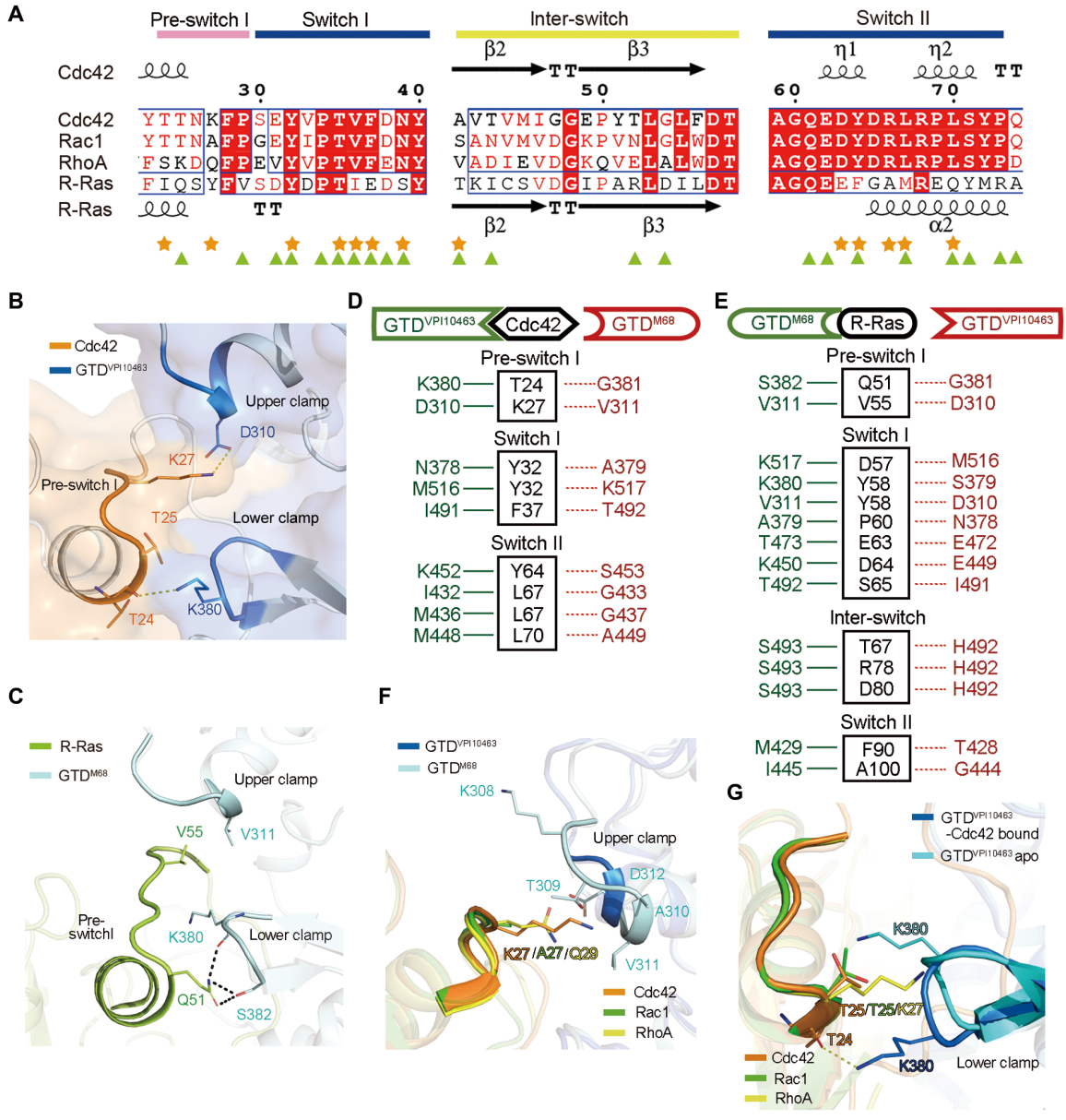

Fig. 4. Structural basis underlying selective targeting of the GTD toward Rho or R-Ras. (**A**) Amino acid sequence alignment among human Cdc42, Rac1, RhoA, and R-Ras that was prepared using MultAlin (*59*) and ESPript 3.0 (*60*), focusing on the pre-switch I, switch I, inter-switch, and switch II regions. Residue numbers for Cdc42 are shown. The secondary structures of Cdc42 and R-Ras are shown on the top and bottom, respectively. The residues in Cdc42 and R-Ras that directly interact with $GTD^{VPI10463}$ or GTD^{M68} are highlighted with orange stars or green triangles, respectively. (**B**) A molecular clamp in $GTD^{VPI10463}$ grips the pre-switch I of Cdc42. (**C**) The molecular clamp in GTD^{M68} selectively interacts with the pre-switch I of R-Ras. (**D**) Strain-specific Cdc42-binding residues in $GTD^{VPI10463}$ are listed in green, while the equivalent residues in GTD^{M68} are listed in red. (**E**) Strain-specific R-Ras–binding residues in GTD^{M68} are listed in green, while the equivalent residues in $GTD^{VPI10463}$ are listed in red. (**F**) The upper clamp in GTD^{M68} (pale cyan) is more compatible to Rac1 that has a small amino acid A27 in this region, while $GTD^{VPI10463}$ (blue) could accommodate Rac1, Cdc42, and RhoA. The structures of Rac1•GDP (PDB: 5N6O, green) and RhoA•GDP (PDB: 1FTN, yellow) were superimposed to the $GTD^{VPI10463}$-bound Cdc42 (orange). (**G**) The lower clamp of $GTD^{VPI10463}$ changes its conformation to recognize the pre-switch I of Rho GTPases.

Although all the GTD mutations discussed above were designed to disrupt its binding to GTPases, some residues may also be involved in its glycohydrolase function. Therefore, we further examined the UDP-glucose hydrolase activity for all the GTD mutants using the UDP-Glo assay. We found that $GTD^{I435G/M436G}$, GTD^{I466G}, $GTD^{I382G/I383G/I466G}$, $GTD^{P471G/I491G}$, GTD^{5MA}, and GTD^{5MB} displayed decreased glycohydrolase activities, while the other mutants showed comparable activity to the WT GTD (fig. S5, D and E, and table S3). Structural analyses showed that residues I383, I466, and P471 help to accommodate the glucose moiety (*30*), which may account for the impaired hydrolase activities when some of these residues were mutated. However, we also observed an unexpected ~5-fold decreased glycohydrolase activity for $GTD^{I435G/M436G}$, which carries mutations on the α16 helix that are far away from the UDP-glucose–binding site. These findings suggest that the in vitro glycohydrolase activity of the GTD in general is very sensitive to

mutagenesis, although all the GTD mutants reported here did not affect GTD folding and stability (figs. S4 and S5C).

TcdB variants could be classified into two groups with different GTPase specificities

Our structural studies reveal four GTD-binding regions in Rho and R-Ras, including switch I, switch II, pre-switch I, and inter-switch (Fig. 4A). As Rho and R-Ras represent two distinct groups in the Ras superfamily, the primary sequences in these four GTD-binding areas are largely conserved within the Rho members but different between Rho and R-Ras (Fig. 4A and fig. S7). Accordingly, structural and sequence analysis showed that GTD^{VPI10463} and GTD^{M68} exploit unique sets of amino acids to preferentially recognize these regions on Rho or R-Ras, respectively (Fig. 4, D and E, and fig. S8).

For example, GTD^{M68}-V311 forms a hydrophobic interaction with R-Ras-V55 on the pre-switch region, which would be abolished by D310 of GTD^{VPI10463}, while two hydrogen bonds formed between the side chain of GTD^{M68}-S382 and R-Ras-Q51 in the pre-switch would be lost with a GTD^{VPI10463}-like G381 (Fig. 4, D and E). Many side-chain–mediated interactions that GTD^{M68} uses to recognize the switch I of R-Ras would be lost if these residues are replaced by the corresponding positions on GTD^{VPI10463}: (i) GTD^{M68}-K380 contacts the main chain of R-Ras-Y58 through its extended side chain, while the equivalent GTD^{VPI10463}-S379 cannot; (ii) GTD^{M68}-T473 forms a hydrogen bond with R-Ras-E63, which would be lost if replaced with the corresponding E472 of GTD^{VPI10463}; (iii) a salt bridge between GTD^{M68}-K450 and R-Ras-D64 would be lost if replaced by E449 of GTD^{VPI10463}; and (iv) E472 and E449 of GTD^{VPI10463} create a negatively charged local surface that may conflict with E63 and D64 on the switch I of R-Ras. Another example involves how GTD^{M68} and GTD^{VPI10463} differently recognize the switch II of Rho and R-Ras: (i) M429 and I445 in the α16–17 helices of GTD^{M68} favorably interact with F90 and A100 in the switch II of R-Ras, which would be weakened with the equivalent T428 and G444 of GTD^{VPI10463}; (ii) residues I432, I435, M436, M447, and M448 in the α16–17 helices of GTD^{VPI10463} form a hydrophobic pocket to accommodate residues L67 and L70 of Cdc42. However, these residues are replaced with G433, L436, G437, I448, and A449, respectively, on GTD^{M68}, which would weaken the interactions between GTD^{M68} and Rho proteins. Together, these findings suggest that the GTD variants may have developed adaptive mutations to differentiate unique sequences of Rho or R-Ras in these four GTD-binding areas and, therefore, selectively target Rho or R-Ras.

To understand how these structural differences exemplified by GTD^{VPI10463} and GTD^{M68} are related to the evolution of diverse TcdB variants, we carried out structure-based sequence analyses among all known TcdB variants available in DiffBase, which have been classified into 12 subfamilies (B1 to B12) (fig. S8) (*18*). We found that all these TcdB variants could be classified into two distinct groups based on their sequences in the GTPase-binding areas. Specifically, characteristic Rho-binding residues are conserved not only in other members of the same subfamily of TcdB^{VPI10463} (B1) but also in members of the B2, B5, B6, B9, B10, B11, and B12 subfamilies, while the R-Ras–binding residues are highly conserved in the B3 (including M68), B4, B7, and B8 subfamilies. Therefore, TcdB seems to have branched into two distinct groups during evolution that have developed two distinct sets of amino acids in their GTPase-binding areas to selectively recognize Rho or R-Ras. We propose to name them the RhoA group and R-Ras group, respectively, based on their preferred substrates, which cause two distinct types of cytopathic effects as reported in prior studies. We envision that these signature sequences in the GTD can be used to predict substrate specificity and pathogenicity of new *C. difficile* clinical strains that will emerge in the future.

To experimentally verify the specific pair-wise recognition between the GTD and its preferred substrate, we first produced a series of chimeric GTD constructs by swapping the GTPase-binding modules between TcdB^{VPI10463} and TcdB^{M68} and then examined how these chimeras change their glucosyltransferase activity toward Rho or R-Ras (Fig. 5A). Specifically, we designed three groups of GTD chimeras whose switch II–, switch I–, or the inter-switch–binding areas were swapped. We confirmed that all these mutations do not affect GTD folding and stability (figs. S4 and S9C), and they are active for UDP-glucose binding and hydrolysis (fig. S9, D and E). We then examined the glucosyltransferase activity of these chimeras against Rho or R-Ras (Fig. 5). In this assay, the lysate of HeLa cells was first treated with the WT GTD and these chimeras, and the unglucosylated RhoA, Rac1/Cdc42, or R-Ras was pulled down by the RhoA effector human Rhotekin (*14*, *22*), Rac1/Cdc42 effector human p21-activated kinase 1 (PAK1) (*14*, *22*), or R-Ras effector Raf1 (*44*), respectively. Since glucosylation of Rho/R-Ras GTPases inhibits their binding to these effector proteins, the fractions of the unglucosylated RhoA, Rac1/Cdc42, or R-Ras that are pulled down by the corresponding effectors reflect the activities of the GTD variants being examined.

We found that all three GTD^{VPI10463} mutants carrying the M68-like switch II–binding site (GTD^{VPI10463}-α16^{M68}, GTD^{VPI10463}-α17^{M68}, and GTD^{VPI10463}-α16/17^{M68}) showed clearly decreased glucosyltransferase activity against three Rho GTPases when compared to the WT GTD^{VPI10463} (Fig. 5, B and C, and fig. S9, A and B). Meanwhile, GTD^{M68}-α16/17^{VPI10463} lost its ability to modify R-Ras. However, it was almost fully active toward Rac1 and partially active toward Cdc42 but barely targeting RhoA (Fig. 5, E and F, and fig. S9, A and B). These results demonstrate that the signature sequences in the α16–17 helices of GTD^{VPI10463} and GTD^{M68} play a key role in differentiating Rho and R-Ras.

When T473 and K450 of GTD^{M68} that favorably interact with the switch I of R-Ras are replaced with the equivalent residue Glu on GTD^{VPI10463}, GTD$^{M68\text{-}T473E/K450E}$ displayed decreased glucosyltransferase ability for R-Ras, while its activity toward Cdc42 was unchanged (Fig. 5, E and F). Nevertheless, the unexpected decrease of its activity toward Rac1 cannot be readily explained on the basis of the structure. In another test, when the R-Ras inter-switch–binding region of GTD^{M68} was swapped with GTD^{VPI10463}-like residues, GTD^{M68}-Inter^{VPI10463} exhibited reduced activity toward R-Ras (Fig. 5). GTD^{M68}-Inter^{VPI10463} showed WT-like activity toward Rac1, but decreased activity against Cdc42 (Fig. 5, E and F, and fig. S9, A and B), suggesting that the inter-switch region on Rho proteins may also participate in binding with GTD^{M68}.

Last, we examined how disrupting GTPase recognition would affect the cytopathic toxicity of the full-length TcdB. As GTD^{VPI10463}-α16/17^{M68} (mutant #4 in Fig. 5) displayed a decreased glucosyltransferase activity but maintained a WT-like hydrolase activity, we incorporated this GTD mutant into the holotoxin. On the basis of the cell-rounding assay, we found that TcdB^{VPI10463}-α16/17^{M68} displayed a drastically decreased cytopathic toxicity: The toxin concentration that induced 50% of the cells to become round (CR_{50}) is ~10.8 ± 5.33 nM, which is ~180,000-fold higher than that of the WT TcdB

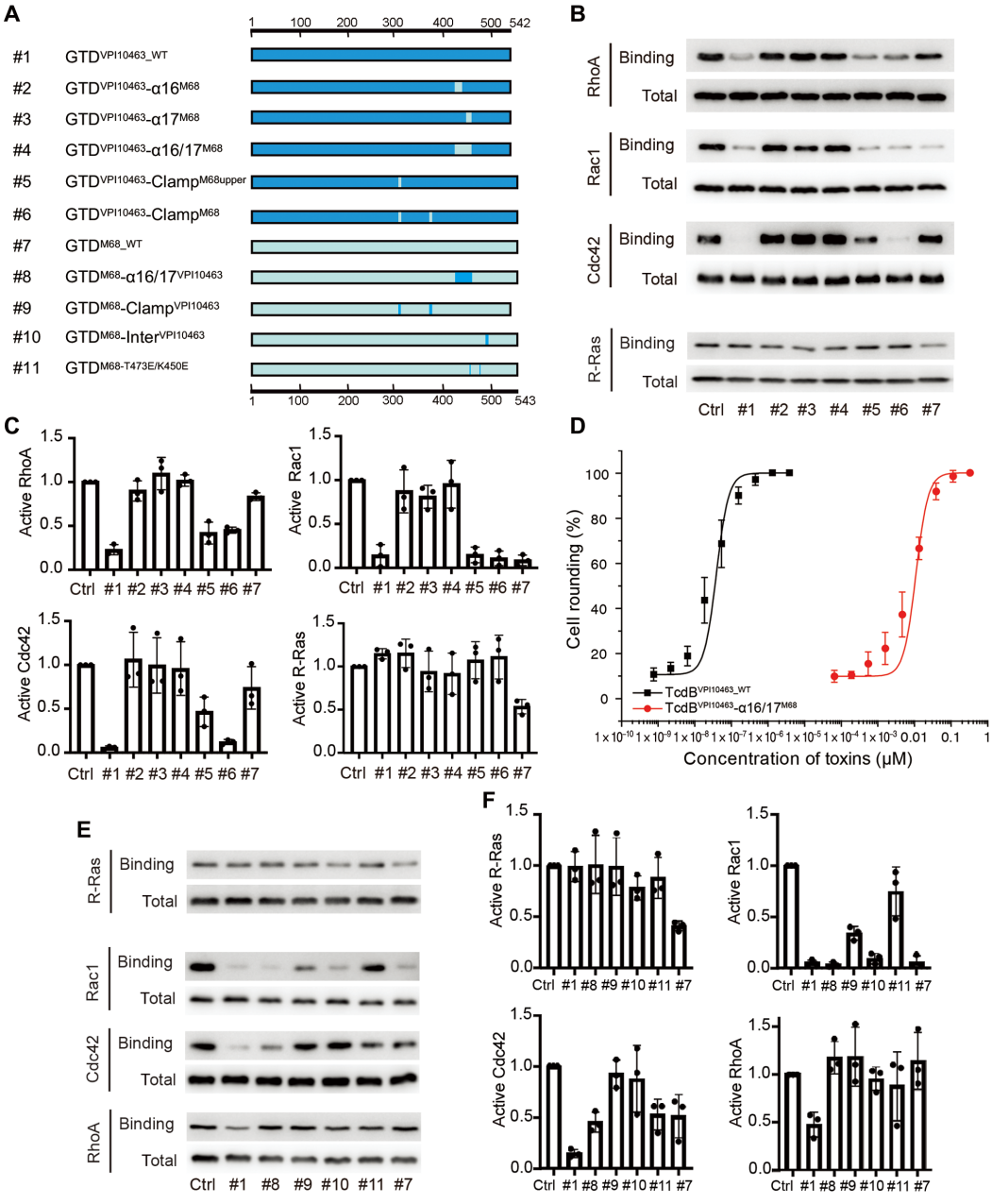

Fig. 5. Mutagenesis studies to examine the structural determinants in the GTD that modulate its substrate specificity. (**A**) Schematic drawing of the designs of GTD chimeric mutants, where the sequences of GTD^{VPI10463} and GTD^{M68} are shown in marine or pale cyan, respectively. Mutant #2: GTD^{VPI10463}-α16^{M68} (GTD^{VPI10463} T428–E438 was replaced with GTD^{M68} M429–I439); #3: GTD^{VPI10463}-α17^{M68} (GTD^{VPI10463} G444–K452 was replaced with GTD^{M68} I445–S453); #4: GTD^{VPI10463}-α16/17^{M68} (GTD^{VPI10463} T428–K452 was replaced with GTD^{M68} M429–S453); #5: GTD^{VPI10463}-Clamp^{M68upper} (GTD^{VPI10463} T308–F311 was replaced with GTD^{M68} K308–D312); #6: GTD^{VPI10463}-Clamp^{M68} (GTD^{VPI10463} T308–F311 and N378–G381 were replaced with GTD^{M68} K308–D312 and A379–S382); #8: GTD^{M68}-α16/17^{VPI10463} (GTD^{M68} M429–S453 was replaced with GTD^{VPI10463} T428–K452); #9: GTD^{M68}-Clamp^{VPI10463} (GTD^{M68} K308–D312 and A379–S382 were replaced with GTD^{VPI10463} T308–F311 and N378–G381); #10: GTD^{M68}-Inter^{VPI10463} (GTD^{M68} D491–L495 was replaced with GTD^{VPI10463} N490–I494); and #11: GTD$^{M68\text{-}T473E/K450E}$. (**B**) Biochemical characterization of substrate specificity for rationally designed GTD mutants based on GTD^{VPI10463}. Rhotekin-RBD, PAK1-RBD, and Raf1-RBD were used to pull down exogenously expressed substrates in HEK 293T cell lysates that were treated by GTD^{VPI10463} variants. Rhotekin-RBD specifically interacts with active RhoA and PAK1-RBD with active Rac1 and Cdc42, while Raf1-RBD interacts with active R-Ras. (**C**) Quantitative analysis of immunoblots in (B). Proportion of active Rho/R-Ras was obtained by dividing the RBD-bound substrates with the total Rho/R-Ras and normalized to the control. (**D**) The cytotoxicity of WT TcdB^{VPI10463} and TcdB^{VPI10463}-α16/17^{M68} was quantified using the cytopathic cell-rounding assay on HeLa cells. (**E**) Biochemical characterization of substrate specificity for rationally designed GTD mutants based on GTD^{M68}. (**F**) Quantitative analysis of immunoblots in (E). Proportion of active Rho/R-Ras was obtained by dividing the RBD-bound substrates with the total Rho/R-Ras and normalized to the control. All data are presented as means ± SD, $n = 3$.

at ~5.9 ± 2.0 × 10^{-2} pM (Fig. 5D). This finding demonstrates that GTPase recognition is crucial for TcdB's cytopathic toxicity and also suggests a strategy to neutralize TcdB by pharmacologically disrupting the GTD-GTPase recognition.

Structural basis for GTD variants' preferences toward different Rho proteins

Given the different substrate specificities between the RhoA and R-Ras group of GTDs, it is intriguing that Rac1 is a good substrate for both groups (*21*, *22*) (Fig. 5A). So, how do the GTDs in the R-Ras group manage to preferentially recognize Rac1 but not the closely related Cdc42 or RhoA? Guided by the crystal structures, we found that the pre-switch I region, which is gripped by a molecular clamp in the GTD, has distinct sequences among Rho GTPases (Cdc42: T^{24}TNK^{27}; Rac1: T^{24}TNA^{27}; RhoA: S^{26}KDQ^{29}), while all other GTD-binding regions in switch I and II are identical within the Rho family (Fig. 4A and fig. S7). Notably, GTD in the R-Ras group has one extra Lys residue inserted in the upper clamp (e.g., K308 in GTD-M68, VPI1470, and 8864) when compared to that in the RhoA group (fig. S8). The large side chain of the inserted Lys in the upper clamp would unfavorably interact with the bulky side chains of $K27^{Cdc42}$ or $Q29^{RhoA}$ while better tolerate $A27^{Rac1}$ (Fig. 4F). We envision that this could render Rac1 as a better substrate for the GTD in the R-Ras group. When we replaced the upper clamp of $GTD^{VPI10463}$ with the homologous region in GTD^{M68} (K308–D312) (termed $GTD^{VPI10463}$-$Clamp^{M68upper}$; Fig. 5A), we found that this mutant effectively glucosylated Rac1 but showed decreased activity toward RhoA and Cdc42 (Fig. 5, B and C). Prior studies also found that replacing $A27^{Rac1}$ with a Lys decreased the glucosyltransferase activity of TcdB in the R-Ras group, while a K27A mutation in Cdc42 showed an improved activity (*45*). These results suggest that a Lys insertion in the upper clamp of GTD in the R-Ras family would negatively affect Cdc42/RhoA recognition.

Structural analysis focusing on the lower clamp shows that this region in $GTD^{VPI10463}$ more favorably interacts with the pre-switch I of Rac1 and Cdc42, which has a smaller residue $T25^{Rac1}$ and $T25^{Cdc42}$ as opposed to the bulky $K27^{RhoA}$ (Fig. 4G). This structural finding is consistent with prior studies showing that substitution of $T25^{Rac1}$ with a RhoA-like Lys led to decreased modification of $Rac1^{T25K}$ by TcdB (*45*). Furthermore, our structural modeling based on calculation of quantitative changes in binding affinity caused by sequence variations using the MutaBind server (*46*) showed that the lower clamp of GTD^{M68} (A379–S382) may provide even better binding for Cdc42 in comparison to that of $GTD^{VPI10463}$ (N378–G381) (table S4). To verify this finding, we generated another mutant of $GTD^{VPI10463}$ whose upper and lower clamps were both replaced by the equivalent regions in GTD^{M68} (termed $GTD^{VPI10463}$-$Clamp^{M68}$; Fig. 5A). We found that this mutant displayed a better activity against Cdc42 when compared to $GTD^{VPI10463}$-$Clamp^{M68upper}$ (Fig. 5, B and C), suggesting that the M68-like lower clamp more favorably interacts with Cdc42 than that of $GTD^{VPI10463}$, which may compensate for the unfavorable interactions imposed by the M68-like upper clamp. Rac1 remained as a good substrate for both $GTD^{VPI10463}$-$Clamp^{M68upper}$ and $GTD^{VPI10463}$-$Clamp^{M68}$ as it has smaller residues A27 and T25 in this region. In contrast, both $GTD^{VPI10463}$-$Clamp^{M68upper}$ and $GTD^{VPI10463}$-$Clamp^{M68}$ displayed decreased activity toward RhoA, which was likely due to the bulky side chains of its Q29 and K27 that impose steric tensions to the M68-like upper and lower clamps in the GTD. These findings suggest that, for GTD^{M68}, the favorable interactions between its clamp and the unique pre-switch I in Rac1 may outweigh the unfavorable contribution of its switch I– and switch II–binding areas that are evolved to better recognize R-Ras. Consistent with this notion, the chimera GTD^{M68}-$Clamp^{VPI10463}$ showed decreased activities toward Cdc42, Rac1, and R-Ras (Fig. 5, E and F, and fig. S9, A and B). Together, our data suggest that the clamp of the GTD helps to fine-tune selectivity toward different Rho members via the pre-switch, while the Rho/R-Ras specificity is jointly determined by all GTPase-binding regions on the GTD.

DISCUSSION

Among the four structurally and functionally distinct domains of TcdB, the GTD is the "warhead" that specifically glucosylates the Rho/Ras GTPases. To better understand the function of the GTD and its contribution to the pathogenicity of TcdB, we determined the crystal structure of the GTD from two distinct TcdB variants, $GTD^{VPI10463}$ and GTD^{M68}, in complex with their preferred substrates human Cdc42 and R-Ras, respectively. These two structures reveal a common structural mechanism by which the GTD from diverse TcdB variants recognizes its substrate via the switch I, switch II, and a pre-switch region in the GTPases. Furthermore, we identified selective clustering of adaptive mutations in the GTDs that modulate their specificities toward Rho or R-Ras. On the basis of the signature sequences in the GTPase-binding sites, TcdB variants can be partitioned into two functional groups: The RhoA group includes the B1, B2, B5, B6, B9, B10, B11, and B12 subfamilies of TcdB that selectively target Rho GTPases but not R-Ras, while the B3, B4, B7, and B8 subfamilies of TcdB form the R-Ras group that effectively targets R-Ras and Rac1, Cdc42 to a less extent, but not RhoA. The different GTPase specificities of these two groups of TcdB are correlated to two distinct types of cytopathic effect (*18*, *47*). These signature sequences in the GTD identified here can be used to predict substrate specificity and pathogenicity of *C. difficile* clinical strains and help inform therapeutic strategies targeting specific toxin variants.

To date, the only nonantibiotic treatment option for CDI is a mAb bezlotoxumab, which blocks TcdB binding to its receptor chondroitin sulfate proteoglycan 4 (CSPG4) via an allosteric mechanism (*48*, *49*). However, TcdB becomes inaccessible to antibodies after entering the host cells. We found that mutations that selectively disrupt GTPases binding drastically reduced the cytopathic toxicity of TcdB holotoxin, which is consistent with prior studies showing that a glucosyltransferase-deficient TcdB mutant was atoxic in vivo (*50*). Therefore, the GTD is an ideal molecular target for therapeutic interventions once the toxin is inside the cells, which will directly target the root cause of disease symptoms and cellular damage. The common feature of GTD-Rho/Ras interplay revealed in these studies could inform the development of therapeutic reagents that inhibit Rho/Ras glucosylation via disrupting the GTD-GTPase recognition. Similar strategies could be applied to develop inhibitors against TcdA and other members in the family of large clostridial glucosylating toxins whose GTDs share similar structures, including *Clostridium novyi* α-toxin (Tcnα), *Clostridium sordellii* lethal and hemorrhagic toxins (TcsL and TcsH), and *Clostridium perfringens* toxin (TpeL) (*2*, *51*).

Notably, TcsL (strain 1522) displays a substrate selectivity similar to that of $TcdB^{M68}$ (*13*), and their GTD domains also share high sequence and structural similarities (*32*). We envision that GTD^{TcsL} should adopt a GTD^{TcdB}-like GTPase–binding mode. For example,

the α16–17 helices on GTD^{TcsL} may favor Ras binding over Rho subfamily because most R-Ras switch II–binding residues on GTD^{M68} are conserved in GTD^{TcsL} (fig. S10A). Moreover, the α16–17 helices on GTD^{TcsL} may be less suitable to target Rho proteins as (i) N452^{TcsL} will abolish a cation-pi interaction formed between the corresponding K452^{VPI10463} and Cdc42-Y64, and (ii) residues S432, A436, and S439 of GTD^{TcsL} may weaken the hydrophobic packing with Cdc42 L67 and L70 on switch II when compared to the GTD^{VPI10463}-like residues (fig. S10B). A previous study showed that swapping the α17 helix between GTD^{TcsL} and GTD^{VPI10463} led to a change of their substrate specificities (*12*). The structure analyses show that the Cdc42 switch I–binding residues on GTD^{VPI10463} are more conserved on GTD^{TcsL}, when compared to the R-Ras switch I–binding residues on GTD^{M68} (fig. S10). However, there are many unique GTD^{TcsL} residues on the GTPase-binding interfaces that could create GTD^{TcsL}-specific interactions with GTPases, and the details await further studies. Therefore, the GTD of TcdB provides an important system to study pathogenic bacteria adaptation and evolution, which might facilitate how pathogens respond to environmental changes, such as host-elicited immune response, different host tissues, or use of antibiotics.

MATERIALS AND METHODS

Cloning, expression, and purification of recombinant proteins

The gene encoding GTD^{VPI10463} (residues M1–S542) of TcdB (strain VPI10463) was cloned into a modified pET28a vector with a 6xHis/SUMO (small ubiquitin-like modifier, *Saccharomyces cerevisiae* Smt3p) tag introduced to its N terminus. Human Rac1 (M1–V182) gene was cloned into the pET28a vector with an N-terminal 7xHis tag followed by a thrombin-cleavage site. For the Cdc42^{T35N}–GTD^{VPI10463} fusion protein, GTD^{VPI10463} was covalently linked to the C terminus of Cdc42^{T35N} (I4–P182) through a 16–amino acid peptide linker (LEVLFQGPGTGSVDGG), and the fusion protein was cloned into the pET28a vector with an N-terminal 6xHis/SUMO tag. GTD^{M68} (M1–A543) of TcdB (strain M68) was expressed as described previously (*52*). For the R-Ras^{T61N}–GTD^{M68} fusion protein, GTD^{M68} was covalently linked to the C terminus of human R-Ras^{T61N} (P24–S201) through a 16–amino acid peptide linker (GGSGGSVDGTGSVDGG), and the fusion protein was cloned into the pET28a vector with an N-terminal 6xHis/SUMO tag. All the GTD, Cdc42–GTD^{VPI10463}, and R-Ras–GTD^{M68} mutants were generated by two-step polymerase chain reaction (PCR) and verified by DNA sequencing. TcdB^{VPI10463} holotoxin and TcdB^{VPI10463}-α16/17^{M68} were cloned into a modified pET28a vector with an N-terminal Twin-Strep tag following a PreScission protease-cleavage site and a C-terminal 6xHis tag. The full-length toxins were expressed and purified as described previously (*49*).

The GTD and its mutants, the covalently linked Cdc42^{T35N}–GTD^{VPI10463} and R-Ras^{T61N}–GTD^{M68}, were expressed in *Escherichia coli* strain BL21-Star (DE3) (Invitrogen). Bacteria were cultured at 37°C in LB medium containing kanamycin. The temperature was reduced to 18°C when optical density at 600 nm reached ~0.8. Expression was induced with 1 mM isopropyl-β-D-thiogalactopyranoside (IPTG) and continued at 18°C overnight. Rac1 was expressed using a similar protocol but with 0.1 mM IPTG induction. The cells were harvested by centrifugation and stored at −80°C until use.

The 6xHis/SUMO–tagged GTD and its mutants were purified using Ni^{2+}-NTA (nitrilotriacetic acid; Qiagen) affinity resins in a buffer containing 50 mM tris (pH 7.5), 400 mM NaCl, 5 mM $MnCl_2$, and 40 mM imidazole. The proteins were eluted with a high-imidazole buffer [50 mM tris (pH 7.5), 400 mM NaCl, 5 mM $MnCl_2$, and 300 mM imidazole] and then exchanged into a buffer containing 20 mM Hepes (pH 7.5), 40 mM NaCl, 5 mM $MnCl_2$, and 1 mM TCEP [tris (2-carboxyethyl) phosphine hydrochloride]. After cleaving the His-SUMO tag by SUMO protease, the GTD and its variants were further purified by Mono Q ion-exchange chromatography (GE Healthcare) in a buffer containing 20 mM Hepes (pH 7.5), 40 mM NaCl, 5 mM $MnCl_2$, and 1 mM TCEP using a NaCl gradient. The peak fractions were pooled and subjected to Superdex-200 size exclusion chromatography (SEC; GE Healthcare) in 20 mM Hepes (pH 7.5), 40 mM NaCl, 5 mM $MnCl_2$, and 1 mM TCEP. The purified proteins were frozen in liquid nitrogen and kept at −80°C. For the Cdc42^{T35N}–GTD^{VPI10463} and R-Ras^{T61N}–GTD^{M68} complexes, the purification protocols are similar to that of the GTD, but the final SEC buffer had 20 mM Hepes (pH 7.5), 40 mM NaCl, 5 mM $MnCl_2$, 5 mM $MgCl_2$, 0.05 mM GDP, and 1 mM TCEP. The purified Cdc42^{T35N}–GTD^{VPI10463} and R-Ras^{T61N}–GTD^{M68} complexes were concentrated to ~6 and ~7 mg/ml, respectively, for crystallization.

The 7xHis–tagged Rac1 was purified using Ni^{2+}-NTA (Qiagen) affinity resins in a buffer containing 50 mM tris (pH 7.5), 400 mM NaCl, 5 mM $MgCl_2$, 0.05 mM GDP, and 40 mM imidazole. Rac1 was eluted with a high-imidazole buffer [50 mM tris (pH 7.5), 400 mM NaCl, 5 mM $MgCl_2$, 0.05 mM GDP, and 300 mM imidazole]; further purified by Mono Q ion-exchange and Superdex-200 SEC (GE Healthcare) in 20 mM Hepes (pH 7.5), 40 mM NaCl, 5 mM $MgCl_2$, 0.05 mM GDP, and 1 mM TCEP; and then frozen in liquid nitrogen and kept at −80°C.

Crystallization

Initial crystallization screening of the Cdc42^{T35N}–GTD^{VPI10463} and the R-Ras^{T61N}–GTD^{M68} complexes in the presence of 5 mM UDP-glucose was carried out at 18°C using a Gryphon crystallization robot (Art Robbins Instruments) with commercial high-throughput crystallization screening kits from Hampton Research and Qiagen. Extensive manual optimizations were then performed at 18°C using the hanging-drop vapor-diffusion method when proteins were mixed with reservoir solution at 1:1 ratio. Streak-seeding was necessary to obtain single crystals suitable for x-ray diffraction. The best crystals for the Cdc42^{T35N}–GTD^{VPI10463} complex were obtained in a mother liquor containing 0.1 M sodium cacodylate (pH 6.6), 2.4 M ammonium sulfate, and 2.5% (v/v) Jeffamine M-600 (pH 7.0), and the crystals were cryo-protected in the mother liquor supplemented with an additional 1.5 M lithium sulfate. The best crystals for the Ras^{T61N}–GTD^{M68} complex were grown in a condition containing 0.2 M ammonium acetate, 0.1 M sodium citrate tribasic dihydrate (pH 4.8), and 17% polyethylene glycol 4000, and the crystals were cryo-protected in the mother liquor supplemented with an additional 25% (v/v) ethylene glycerol.

Data collection and structure determination

The x-ray diffraction data were collected at 100 K at the NE-CAT beamline 24-ID-C, Advanced Photon Source. The data were processed with XDS software as implemented in RAPD (https://github.com/RAPD/RAPD) (*53*). For the Cdc42^{T35N}–GTD^{VPI10463} complex, the structure was solved by molecular replacement using GTD^{VPI10463} (PDB: 2BVM) (*30*) and Cdc42 (PDB: 2WMN) (*54*) as the search models. One Cdc42^{T35N}–GTD^{VPI10463} molecule could be positioned in the

asymmetric unit using PHENIX.Phaser (*55*). For the R-Ras^{T61N}–GTD^{M68} complex, the structure was solved by molecular replacement using GTD^{M68} (PDB: 6OQ7) (*34*) and R-Ras (PDB: 2FN4) as the search models. Two R-Ras^{T61N}–GTD^{M68} molecules were positioned in the asymmetric unit using PHENIX.Phaser (*55*). The initial atomic models were refined with PHENIX.Refinement (*55*). Further structural modeling and refinement were carried out iteratively using COOT (*56*) and Phenix.Refinement (*55*) or Refmac5 refinement (*57*). All the refinement progress was monitored with the free R value using a 5% randomly selected test set. The structures were validated through the MolProbity (*58*). Data collection and structural refinement statistics are listed in table S1. All structure figures were prepared with PyMOL (DeLano Scientific).

Glucosyltransferase assay

For each reaction, the recombinant Rac1 (1 μM) was incubated with 10 nM GTD (WT or the mutants) and 10 μM UDP-glucose in a 20-μl buffer containing 50 mM Hepes (pH 7.5), 100 mM KCl, 2 mM $MgCl_2$, 1 mM $MnCl_2$, 10 μM GDP, and bovine serum albumin (0.1 mg/ml) for 60 min at room temperature. The reactions were stopped by adding 2× SDS loading buffer and boiling at 100°C. An equal amount of Rac1 from each reaction was loaded and analyzed by SDS–polyacrylamide gel electrophoresis (SDS-PAGE). Following electrophoresis, samples were transferred to nitrocellulose membranes and blocked with 5% milk/phosphate-buffered saline and 0.05% Tween 20 (PBST) and then probed with a 1/4000 dilution of the anti-Rac1 antibodies mAb 102 (BD Biosciences) or mAb 23A8 (MilliporeSigma). After an overnight incubation with the primary antibody, the blots were washed with PBST buffer and incubated with a 1/4000 dilution of an anti-mouse antibody conjugated with horseradish peroxidase for 60 min. Chemiluminescent detection was carried out using the enhanced chemiluminescence substrate kit (Thermo Fisher Scientific) and recorded on ChemiDoc Molecular Imager (Bio-Rad).

Protein-melting assay

The thermal stability of the GTD variants was measured using a fluorescence-based thermal shift assay on a StepOne real-time PCR machine (Life Technologies). Each protein (~0.5 mg/ml) was mixed with the fluorescent dye SYPRO Orange (Sigma-Aldrich) and heated from 25° to 90°C in a linear ramp. The midpoint of the protein-melting curve (T_m) was determined using the analysis software provided by the instrument manufacturer. Data obtained from three independent experiments were averaged to generate the bar graph.

Cytopathic assay

The purified WT and mutant GTDs were transfected into HeLa cell via the Lipofectamine CRISPRMAX Cas9 Transfection Reagent from Thermo Fisher Scientific. The transfection was performed in coherence to the protocol provided by the manufacturer. HeLa cells at 5×10^4 per well were seeded into 24-well plates for overnight culture. For each well, we prepared solutions in tube 1 that contained 25 μl of Opti-MEM medium, 1250 ng of GTD, and 2.5 μl of Cas9 Plus Reagent and in tube 2 that contained 25 μl of Opti-MEM medium and 1.5 μl of CRISPRMAX reagent. We immediately added the solution from tube 1 to tube 2 and then mixed well. We incubated the complex for 10 min at room temperature then added all 50 μl of solution to the cells. The phase-contrast images of cells were taken at the indicated time (Olympus IX51; 10× objective). To test the full-length TcdB, HeLa cells were exposed to WT TcdB^{VPI10463} or TcdB^{VPI10463}-α16/17^{M68} at indicated concentrations, and cells were imaged after overnight. Round-shaped and normal-shaped cells were counted manually. The percentage of round-shaped cells was analyzed using the OriginPro (OriginLab, v8.5) and Excel (Microsoft, 2007).

GTPase effector pull-down assay

Myc-tagged RhoA, Rac1, Cdc42, and hemagglutinin (HA)–tagged R-Ras were exogenously expressed in human embryonic kidney (HEK) 293T cells on 10-cm cell culture dishes. Cells were harvested 48 hours after transfection and lysed in 3-ml lysis buffer (PBS containing 1% Triton X-100, 0.1% SDS, 1× protease inhibitor, and phosphatase inhibitor). Cell lysates were then aliquoted into 1.5-ml Eppendorf tubes and treated with 0.2 μM GTDs for 30 min at 37°C. Glutathione beads (30 μl) preincubated with glutathione *S*-transferase–tagged Rhotekin-RBD (residues 7 to 89), PAK1-RBD (residues 70 to 117), or Raf1-RBD (residues 1 to 149) were then added into each tube for incubation with gentle rotation for 30 min at 4°C. Beads were then washed three times with PBS and boiled in 30 μl of SDS-PAGE loading buffer. Cell lysates in each tube before GTD treatment were used as total input. Samples were subjected to SDS-PAGE analysis and Western blot. Rho/R-Ras GTPases were detected with anti-myc and anti-HA antibodies.

UDP-Glo UDP-glucose hydrolase assay

The hydrolase assay was performed following the manufacturer's instruction (Promega). Briefly, 100 nM GTD and the mutations were incubated with 100 μM UDP-glucose in the hydrolase buffer [50 mM Hepes (pH 7.5), 100 mM KCl, 2 mM $MgCl_2$, 1 mM $MnCl_2$, and bovine serum albumin (0.1 mg/ml)] with a final volume of 20 μl. Reactions were allowed to proceed at room temperature for 15 or 60 min. Then, 10 μl of each reaction was added to a white, polystyrene, 96-well half-area microplate (Corning) containing 10 μl of UDP detection reagent that stopped the hydrolysis reaction. The plates were further incubated at room temperature for 1 hour, and luminescence was then recorded on a PerkinElmer multimode plate reader (EnVision 2015). To determine the kinetic parameters for the initial rate of the glycohydrolase reaction, 100 nM GTD or the mutants were incubated with varying concentrations of UDP-glucose (1.56 to 500 μM) in the hydrolase buffer for 15 min at room temperature. A UDP standard curve was established according to the manufacturer's instructions to determine the conversion factor between the luminescence intensity and the amount of UDP product. The K_m (Michaelis constant) and V_{max} (maximal velocity) values were plotted against substrate UDP-glucose concentrations and fitted to the Michaelis-Menten equation. The data were obtained from three independent experiments.

SUPPLEMENTARY MATERIALS

Supplementary material for this article is available at https://science.org/doi/10.1126/sciadv.abi4582

View/request a protocol for this paper from *Bio-protocol*.

REFERENCES AND NOTES

1. F. C. Lessa, Y. Mu, W. M. Bamberg, Z. G. Beldavs, G. K. Dumyati, J. R. Dunn, M. M. Farley, S. M. Holzbauer, J. I. Meek, E. C. Phipps, L. E. Wilson, L. G. Winston, J. A. Cohen, B. M. Limbago, S. K. Fridkin, D. N. Gerding, L. C. McDonald, Burden of *Clostridium difficile* infection in the United States. *N. Engl. J. Med.* **372**, 825–834 (2015).

2. K. Aktories, C. Schwan, T. Jank, *Clostridium difficile* toxin biology. *Annu. Rev. Microbiol.* **71**, 281–307 (2017).
3. D. Lyras, J. R. O'Connor, P. M. Howarth, S. P. Sambol, G. P. Carter, T. Phumoonna, R. Poon, V. Adams, G. Vedantam, S. Johnson, D. N. Gerding, J. I. Rood, Toxin B is essential for virulence of *Clostridium difficile*. *Nature* **458**, 1176–1179 (2009).
4. D. Drudy, S. Fanning, L. Kyne, Toxin A-negative, toxin B-positive *Clostridium difficile*. *Int. J. Infect. Dis.* **11**, 5–10 (2007).
5. P. Yuan, H. Zhang, C. Cai, S. Zhu, Y. Zhou, X. Yang, R. He, C. Li, S. Guo, S. Li, T. Huang, G. Perez-Cordon, H. Feng, W. Wei, Chondroitin sulfate proteoglycan 4 functions as the cellular receptor for *Clostridium difficile* toxin B. *Cell Res.* **25**, 157–168 (2015).
6. P. Chen, L. Tao, Z. Liu, M. Dong, R. Jin, Structural insight into Wnt signaling inhibition by *Clostridium difficile* toxin B. *FEBS J.* **286**, 874–881 (2019).
7. L. Tao, J. Zhang, P. Meraner, A. Tovaglieri, X. Wu, R. Gerhard, X. Zhang, W. B. Stallcup, J. Miao, X. He, J. G. Hurdle, D. T. Breault, A. L. Brass, M. Dong, Frizzled proteins are colonic epithelial receptors for *C. difficile* toxin B. *Nature* **538**, 350–355 (2016).
8. P. Chen, L. Tao, T. Wang, J. Zhang, A. He, K. H. Lam, Z. Liu, X. He, K. Perry, M. Dong, R. Jin, Structural basis for recognition of frizzled proteins by *Clostridium difficile* toxin B. *Science* **360**, 664–669 (2018).
9. Z. Zhang, M. Park, J. Tam, A. Auger, G. L. Beilhartz, D. B. Lacy, R. A. Melnyk, Translocation domain mutations affecting cellular toxicity identify the *Clostridium difficile* toxin B pore. *Proc. Natl. Acad. Sci. U.S.A.* **111**, 3721–3726 (2014).
10. M. Qa'Dan, L. M. Spyres, J. D. Ballard, pH-induced conformational changes in *Clostridium difficile* toxin B. *Infect. Immun.* **68**, 2470–2474 (2000).
11. I. Just, J. Selzer, M. Wilm, C. von Eichel-Streiber, M. Mann, K. Aktories, Glucosylation of Rho proteins by Clostridium difficile toxin B. *Nature* **375**, 500–503 (1995).
12. T. Jank, T. Giesemann, K. Aktories, Clostridium difficile glucosyltransferase toxin B-essential amino acids for substrate binding. *J. Biol. Chem.* **282**, 35222–35231 (2007).
13. E. Chaves-Olarte, P. Low, E. Freer, T. Norlin, M. Weidmann, C. von Eichel-Streiber, M. Thelestam, A novel cytotoxin from Clostridium difficile serogroup F is a functional hybrid between two other large clostridial cytotoxins. *J. Biol. Chem.* **274**, 11046–11052 (1999).
14. E. Chaves-Olarte, E. Freer, A. Parra, C. Guzman-Verri, E. Moreno, M. Thelestam, R-Ras glucosylation and transient RhoA activation determine the cytopathic effect produced by toxin B variants from toxin A-negative strains of Clostridium difficile. *J. Biol. Chem.* **278**, 7956–7963 (2003).
15. H. Genth, S. Pauillac, I. Schelle, P. Bouvet, C. Bouchier, C. Varela-Chavez, I. Just, M. R. Popoff, Haemorrhagic toxin and lethal toxin from Clostridium sordellii strain vpi9048: Molecular characterization and comparative analysis of substrate specificity of the large clostridial glucosylating toxins. *Cell. Microbiol.* **16**, 1706–1721 (2014).
16. E. Lemichez, K. Aktories, Hijacking of Rho GTPases during bacterial infection. *Exp. Cell Res.* **319**, 2329–2336 (2013).
17. P. Sehr, G. Joseph, H. Genth, I. Just, E. Pick, K. Aktories, Glucosylation and ADP ribosylation of rho proteins: Effects on nucleotide binding, GTPase activity, and effector coupling. *Biochemistry* **37**, 5296–5304 (1998).
18. M. J. Mansfield, B. J. Tremblay, J. Zeng, X. Wei, H. Hodgins, J. Worley, L. Bry, M. Dong, A. C. Doxey, Phylogenomics of 8,839 *Clostridioides difficile* genomes reveals recombination-driven evolution and diversification of toxin A and B. *PLOS Pathog.* **16**, e1009181 (2020).
19. Z. Li, K. Lee, U. Rajyaguru, C. H. Jones, S. Janezic, M. Rupnik, A. S. Anderson, P. Liberator, Ribotype classification of *Clostridioides difficile* isolates is not predictive of the amino acid sequence diversity of the toxin virulence factors TcdA and TcdB. *Front. Microbiol.* **11**, 1310 (2020).
20. E. Shen, K. Zhu, D. Li, Z. Pan, Y. Luo, Q. Bian, L. He, X. Song, Y. Zhen, D. Jin, L. Tao, Subtyping analysis reveals new variants and accelerated evolution of *Clostridioides difficile* toxin B. *Commun. Biol.* **3**, 347 (2020).
21. J. Huelsenbeck, S. Dreger, R. Gerhard, H. Barth, I. Just, H. Genth, Difference in the cytotoxic effects of toxin B from *Clostridium difficile* strain VPI 10463 and toxin B from variant *Clostridium difficile* strain 1470. *Infect. Immun.* **75**, 801–809 (2007).
22. C. Quesada-Gomez, D. Lopez-Urena, N. Chumbler, H. K. Kroh, C. Castro-Pena, C. Rodriguez, J. Orozco-Aguilar, S. Gonzalez-Camacho, A. Rucavado, C. Guzman-Verri, T. D. Lawley, D. B. Lacy, E. Chaves-Olarte, Analysis of TcdB proteins within the hypervirulent clade 2 reveals an impact of RhoA glucosylation on *Clostridium difficile* proinflammatory activities. *Infect. Immun.* **84**, 856–865 (2016).
23. A. B. Jaffe, A. Hall, Rho GTPases: Biochemistry and biology. *Annu. Rev. Cell Dev. Biol.* **21**, 247–269 (2005).
24. M. Lehto, M. I. Mayranpaa, T. Pellinen, P. Ihalmo, S. Lehtonen, P. T. Kovanen, P. H. Groop, J. Ivaska, V. M. Olkkonen, The R-Ras interaction partner ORP3 regulates cell adhesion. *J. Cell Sci.* **121**, 695–705 (2008).
25. T. Sethi, M. H. Ginsberg, J. Downward, P. E. Hughes, The small GTP-binding protein R-Ras can influence integrin activation by antagonizing a Ras/Raf-initiated integrin suppression pathway. *Mol. Biol. Cell* **10**, 1799–1809 (1999).
26. M. Komatsu, E. Ruoslahti, R-Ras is a global regulator of vascular regeneration that suppresses intimal hyperplasia and tumor angiogenesis. *Nat. Med.* **11**, 1346–1350 (2005).
27. C. Depitre, M. Delmee, V. Avesani, R. L'Haridon, A. Roels, M. Popoff, G. Corthier, Serogroup F strains of *Clostridium difficile* produce toxin B but not toxin A. *J. Med. Microbiol.* **38**, 434–441 (1993).
28. G. Yao, S. Zhang, S. Mahrhold, K. H. Lam, D. Stern, K. Bagramyan, K. Perry, M. Kalkum, A. Rummel, M. Dong, R. Jin, N-linked glycosylation of SV2 is required for binding and uptake of botulinum neurotoxin A. *Nat. Struct. Mol. Biol.* **23**, 656–662 (2016).
29. R. Jin, A. Rummel, T. Binz, A. T. Brunger, Botulinum neurotoxin B recognizes its protein receptor with high affinity and specificity. *Nature* **444**, 1092–1095 (2006).
30. D. J. Reinert, T. Jank, K. Aktories, G. E. Schulz, Structural basis for the function of *Clostridium difficile* toxin B. *J. Mol. Biol.* **351**, 973–981 (2005).
31. J. W. Alvin, D. B. Lacy, *Clostridium difficile* toxin glucosyltransferase domains in complex with a non-hydrolyzable UDP-glucose analogue. *J. Struct. Biol.* **198**, 203–209 (2017).
32. M. O. Ziegler, T. Jank, K. Aktories, G. E. Schulz, Conformational changes and reaction of clostridial glycosylating toxins. *J. Mol. Biol.* **377**, 1346–1356 (2008).
33. R. N. Pruitt, N. M. Chumbler, S. A. Rutherford, M. A. Farrow, D. B. Friedman, B. Spiller, D. B. Lacy, Structural determinants of *Clostridium difficile* toxin A glucosyltransferase activity. *J. Biol. Chem.* **287**, 8013–8020 (2012).
34. P. Chen, K. H. Lam, Z. Liu, F. A. Mindlin, B. Chen, C. B. Gutierrez, L. Huang, Y. Zhang, T. Hamza, H. Feng, T. Matsui, M. E. Bowen, K. Perry, R. Jin, Structure of the full-length *Clostridium difficile* toxin B. *Nat. Struct. Mol. Biol.* **26**, 712–719 (2019).
35. M. J. Phillips, G. Calero, B. Chan, S. Ramachandran, R. A. Cerione, Effector proteins exert an important influence on the signaling-active state of the small GTPase Cdc42. *J. Biol. Chem.* **283**, 14153–14164 (2008).
36. K. Ihara, S. Muraguchi, M. Kato, T. Shimizu, M. Shirakawa, S. Kuroda, K. Kaibuchi, T. Hakoshima, Crystal structure of human RhoA in a dominantly active form complexed with a GTP analogue. *J. Biol. Chem.* **273**, 9656–9666 (1998).
37. Y. Wei, Y. Zhang, U. Derewenda, X. Liu, W. Minor, R. K. Nakamoto, A. V. Somlyo, A. P. Somlyo, Z. S. Derewenda, Crystal structure of RhoA-GDP and its functional implications. *Nat. Struct. Biol.* **4**, 699–703 (1997).
38. M. Hirshberg, R. W. Stockley, G. Dodson, M. R. Webb, The crystal structure of human rac1, a member of the rho-family complexed with a GTP analogue. *Nat. Struct. Biol.* **4**, 147–152 (1997).
39. Y. Ferrandez, W. Zhang, F. Peurois, L. Akendengue, A. Blangy, M. Zeghouf, J. Cherfils, Allosteric inhibition of the guanine nucleotide exchange factor DOCK5 by a small molecule. *Sci. Rep.* **7**, 14409 (2017).
40. G. R. Hoffman, N. Nassar, R. A. Cerione, Structure of the Rho family GTP-binding protein Cdc42 in complex with the multifunctional regulator RhoGDI. *Cell* **100**, 345–356 (2000).
41. S. C. Huelsenbeck, I. Klose, M. Reichenbach, J. Huelsenbeck, H. Genth, Distinct kinetics of (H/K/N)Ras glucosylation and Rac1 glucosylation catalysed by Clostridium sordellii lethal toxin. *FEBS Lett.* **583**, 3133–3139 (2009).
42. H. Genth, J. Huelsenbeck, B. Hartmann, F. Hofmann, I. Just, R. Gerhard, Cellular stability of Rho-GTPases glucosylated by Clostridium difficile toxin B. *FEBS Lett.* **580**, 3565–3569 (2006).
43. A. Hall, Rho GTPases and the actin cytoskeleton. *Science* **279**, 509–514 (1998).
44. M. Spaargaren, G. A. Martin, F. McCormick, M. J. Fernandez-Sarabia, J. R. Bischoff, The Ras-related protein R-ras interacts directly with Raf-1 in a GTP-dependent manner. *Biochem. J.* **300** (Pt. 2), 303–307 (1994).
45. S. Muller, C. von Eichel-Streiber, M. Moos, Impact of amino acids 22-27 of Rho-subfamily GTPases on glucosylation by the large clostridial cytotoxins TcsL-1522, TcdB-1470 and TcdB-8864. *Eur. J. Biochem.* **266**, 1073–1080 (1999).
46. M. Li, F. L. Simonetti, A. Goncearenco, A. R. Panchenko, MutaBind estimates and interprets the effects of sequence variants on protein-protein interactions. *Nucleic Acids Res.* **44**, W494–W501 (2016).
47. G. Ramirez-Vargas, D. Lopez-Urena, A. Badilla, J. Orozco-Aguilar, T. Murillo, P. Rojas, T. Riedel, J. Overmann, G. Gonzalez, E. Chaves-Olarte, C. Quesada-Gomez, C. Rodriguez, Novel clade C-I *Clostridium difficile* strains escape diagnostic tests, differ in pathogenicity potential and carry toxins on extrachromosomal elements. *Sci. Rep.* **8**, 13951 (2018).
48. P. Orth, L. Xiao, L. D. Hernandez, P. Reichert, P. R. Sheth, M. Beaumont, X. Yang, N. Murgolo, G. Ermakov, E. DiNunzio, F. Racine, J. Karczewski, S. Secore, R. N. Ingram, T. Mayhood, C. Strickland, A. G. Therien, Mechanism of action and epitopes of *Clostridium difficile* toxin B-neutralizing antibody bezlotoxumab revealed by x-ray crystallography. *J. Biol. Chem.* **289**, 18008–18021 (2014).
49. P. Chen, J. Zeng, Z. Liu, H. Thaker, S. Wang, S. Tian, J. Zhang, L. Tao, C. B. Gutierrez, L. Xing, R. Gerhard, L. Huang, M. Dong, R. Jin, Structural basis for CSPG4 as a receptor for TcdB and a therapeutic target in *Clostridioides difficile* infection. *Nat. Commun.* **12**, 3748 (2021).
50. T. W. Bilverstone, M. Garland, R. J. Cave, M. L. Kelly, M. Tholen, D. M. Bouley, P. Kaye, N. P. Minton, M. Bogyo, S. A. Kuehne, R. A. Melnyk, The glucosyltransferase activity of *C. difficile* toxin B is required for disease pathogenesis. *PLOS Pathog.* **16**, e1008852 (2020).

51. I. Just, R. Gerhard, Large clostridial cytotoxins. *Rev. Physiol. Biochem. Pharmacol.* **152**, 23–47 (2004).
52. G. L. Yang, B. P. Zhou, J. F. Wang, X. Y. He, X. M. Sun, W. J. Nie, S. Tzipori, H. P. Feng, Expression of recombinant *Clostridium difficile* toxin A and B in *Bacillus megaterium*. *BMC Microbiol.* **8**, 192 (2008).
53. W. Kabsch, XDS. *Acta Crystallogr. D Biol. Crystallogr.* **66**, 125–132 (2010).
54. J. Yang, Z. Zhang, S. M. Roe, C. J. Marshall, D. Barford, Activation of Rho GTPases by DOCK exchange factors is mediated by a nucleotide sensor. *Science* **325**, 1398–1402 (2009).
55. P. D. Adams, P. V. Afonine, G. Bunkoczi, V. B. Chen, I. W. Davis, N. Echols, J. J. Headd, L. W. Hung, G. J. Kapral, R. W. Grosse-Kunstleve, A. J. McCoy, N. W. Moriarty, R. Oeffner, R. J. Read, D. C. Richardson, J. S. Richardson, T. C. Terwilliger, P. H. Zwart, PHENIX: A comprehensive Python-based system for macromolecular structure solution. *Acta Crystallogr. D Biol. Crystallogr.* **66**, 213–221 (2010).
56. P. Emsley, B. Lohkamp, W. G. Scott, K. Cowtan, Features and development of Coot. *Acta Crystallogr. D Biol. Crystallogr.* **66**, 486–501 (2010).
57. G. N. Murshudov, P. Skubak, A. A. Lebedev, N. S. Pannu, R. A. Steiner, R. A. Nicholls, M. D. Winn, F. Long, A. A. Vagin, REFMAC5 for the refinement of macromolecular crystal structures. *Acta Crystallogr. D* **67**, 355–367 (2011).
58. V. B. Chen, W. B. Arendall III, J. J. Headd, D. A. Keedy, R. M. Immormino, G. J. Kapral, L. W. Murray, J. S. Richardson, D. C. Richardson, MolProbity: All-atom structure validation for macromolecular crystallography. *Acta Crystallogr. D Biol. Crystallogr.* **66**, 12–21 (2010).
59. F. Corpet, Multiple sequence alignment with hierarchical clustering. *Nucleic Acids Res.* **16**, 10881–10890 (1988).
60. X. Robert, P. Gouet, Deciphering key features in protein structures with the new ENDscript server. *Nucleic Acids Res.* **42**, W320–W324 (2014).

Acknowledgments

Funding: This work was partly supported by NIH grants R01AI125704, R21AI139690, and R21AI123920 to R.J.; R01NS080833 and R01AI132387 to M.D.; and R01AI139087 and R21 CA235533 to R.J. and M.D. M.D. holds the Investigator in the Pathogenesis of Infectious Disease award from the Burroughs Wellcome Fund. NE-CAT at the Advanced Photon Source (APS) is supported by a grant from the National Institute of General Medical Sciences (P30 GM124165), and the Eiger 16M detector on the 24-ID-E beamline is funded by an NIH-ORIP HEI grant (S10OD021527). Use of the APS, an Office of Science User Facility operated for the U.S. Department of Energy (DOE) Office of Science by Argonne National Laboratory, was supported by the U.S. DOE under contract no. DE-AC02-06CH11357. **Author contributions:** Conceptualization: Z.L. and R.J. Investigation: Z.L., S.Z., P.C., S.T., J.Z., and K.P. Supervision: M.D. and R.J. Writing—original draft: Z.L. and R.J. Writing—review and editing: Z.L., M.D., and R.J. **Competing interests:** The authors declare that they have no competing interests. **Data and materials availability:** Atomic coordinates and structure factors of the Cdc42^{T35N}–GTD^{VPI10463} and R-Ras^{T61N}–GTD^{M68} complexes have been deposited in the PDB under accession codes 7S0Y and 7S0Z, respectively. The x-ray diffraction data were processed with XDS as implemented in RAPD (https://github.com/RAPD/RAPD). All data needed to evaluate the conclusions in the paper are present in the paper and/or the Supplementary Materials.

Submitted 11 March 2021
Accepted 2 September 2021
Published 22 October 2021
10.1126/sciadv.abi4582

Citation: Z. Liu, S. Zhang, P. Chen, S. Tian, J. Zeng, K. Perry, M. Dong, R. Jin, Structural basis for selective modification of Rho and Ras GTPases by *Clostridioides difficile* toxin B. *Sci. Adv.* **7**, eabi4582 (2021).

ScienceAdvances

Structural basis for selective modification of Rho and Ras GTPases by *Clostridioides difficile* toxin B

Zheng LiuSicai ZhangPeng ChenSonghai TianJi ZengKay PerryMin DongRongsheng Jin

Sci. Adv., 7 (43), eabi4582. • DOI: 10.1126/sciadv.abi4582